

## Article

# Photocatalytic Porous Silica-Based Granular Media for Organic Pollutant Degradation in Industrial Waste-Streams

Hannah M. McIntyre  and Megan L. Hart \* 

University of Missouri—Kansas City, 5110 Rockhill Rd, 352 Flarsheim Hall Kansas City, Kansas City, MO 64110, USA; hmmg2d@umsystem.edu

\* Correspondence: hartme@umsystem.edu; Tel.: +816-235-1270

**Abstract:** Photocatalytic treatment of organic contaminants in industrial wastewaters has gained interest due to their potential for effective degradation. However, photocatalytic slurry reactors are hindered by solution turbidity, dissolved salt content, and absorbance of light. Research presented here introduces the development and application of a novel, photocatalytic, porous silica-based granular media (SGM). SGM retains the cross-linked structure developed during synthesis through a combination of foaming agent addition and activation temperature. The resultant media has a high porosity of 88%, with a specific surface area of  $\sim 150 \text{ m}^2/\text{gram}$ . Photocatalytic capabilities are further enhanced as the resultant structure fixes the photocatalyst within the translucent matrix. SGM is capable of photocatalysis combined with diffusion of nucleophiles, electrophiles, and salts from pore space. The photocatalytic efficiencies of SGM at various silica contents were quantified in batch reactors using methylene blue destruction over time and cycles. Methylene blue concentrations of 10 mg/L were effectively degraded ( $>90\%$ ) within 40 min. This effectiveness was retained over multiple cycles and various methylene blue concentrations. SGM is a passive and cost-effective granular treatment system technology which can translate to other organic contaminants and industrial processes.

**Keywords:** granular photocatalytic material; nucleophile



**Citation:** McIntyre, H.M.; Hart, M.L. Photocatalytic Porous Silica-Based Granular Media for Organic Pollutant Degradation in Industrial Waste-Streams. *Catalysts* **2021**, *11*, 258. <https://doi.org/10.3390/catal11020258>

Academic Editors: Lucyna Bilińska, Marta Gmurek and Agnieszka Ruppert  
Received: 21 January 2021  
Accepted: 12 February 2021  
Published: 15 February 2021

**Publisher's Note:** MDPI stays neutral with regard to jurisdictional claims in published maps and institutional affiliations.



**Copyright:** © 2021 by the authors. Licensee MDPI, Basel, Switzerland. This article is an open access article distributed under the terms and conditions of the Creative Commons Attribution (CC BY) license (<https://creativecommons.org/licenses/by/4.0/>).

## 1. Introduction

As expansions in the textile industry continue, remedial technologies for textile dyes have become very important and in demand [1]. Since the industrial switch from natural dyes to synthetic, over 100,000 synthetic dyes have been produced and are widely associated with water pollution stemming from the discharge of untreated effluents into bodies of water [2–4]. With no requirement for pretreatment of effluent streams, 280,000 tons of dyes per year are discharged as effluent to water ways [5]. Organic dyes contribute to wastewater in various other aspects such as in hair dye [6] leather and paper industries [7], and luminescent solar concentrator (LSC) technologies [8]. Organic chemicals used in dyes are known to be toxic to the environment and cause detrimental health effects in humans, such as respiratory illnesses [9]. Textile dyes are highly soluble, organic compounds that cannot be effectively treated using conventional wastewater treatment technologies. Dye-specific treatment methods include adsorption and electro-chemical destabilization; however, these processes produce concentrated waste streams or additional byproducts which require further treatment or disposal [10]. Degradation of textile dyes by nucleophilic attack has been shown to be a promising method for mineralization of methylene blue as individual components [11,12]. Photocatalytic degradation processes have also shown to be effective in rapidly degrading numerous organic pollutants, including textile dyes [13,14]. Very few existing technologies combine the attacks for an improved treatment.

Photocatalysts are substances which use absorbed light to produce photoexcited electrons. These photoexcited electrons are then transferred from the valence band gap to the conduction band gap [15]. This process generates electron–hole pairs ( $e^-/h^+$ )

which act to reduce and/or oxidize organic compounds and decompose water adjacent to the catalyst surfaces [16–19]. Heterogeneous metal oxides such as  $\text{TiO}_2$ ,  $\text{ZnO}$ ,  $\text{SnO}_2$ , and  $\text{CeO}_2$ , are naturally occurring, abundant, and widely used in photocatalytic applications because of their ability to produce positive electrons holes. While various heterogeneous photocatalysts have been studied and utilized [20–23], titanium dioxide has received the most attention for organic contaminant degradation [24–26]. Titanium dioxide possesses photostability and low toxicity, making it a superior catalyst for organic pollutants [27–29].

Sol-gels form during a chemical reaction, hydrolysis/condensation, between a precursor and water, which promotes a biphasic cross-linking of silica-oxygen bonds to create a stable gel structure. Silica solutions formed during cross-linking of chains convert monomers into a colloidal media that can be further evolved into discrete particles or networked gel semi-solids. Two major families of sol gels exist, xerogels and aerogels which are differentiated based upon the method for extraction of solvent solutions from the network of cross-linked gels. Within both aerogel and xerogel processes, metal oxides are utilized as dispersant aids and as additives to the final gel structure. In particular titanium is used for multiple purposes, but the xerogel sol gel process is widely utilized as a method for producing doped and uniform photocatalysts.

Sol-gel processes are an innovative methodology for developing nanoparticles used for treating emerging contaminants of concern, especially when addressing organics. The sol-gel synthesis process allows for the usage of the anatase phase of titanium dioxide, which has a larger band gap (3.2 eV) than rutile (3.0 eV). A larger band gap has been shown to reduce the light absorbed but increased the oxidation ability of electrons [30]. The photocatalytic capabilities of titanium dioxide can be further enhanced by doping the nanoparticles with various other transition metals such as iron, niobium, and chromium [31]. However, leaching of the doped species often occurs and is cause for concern if dopants are toxic metals such as chromium [32].

One major advantage of incorporating photocatalytic materials within the sol-gel process is the ability to promote an increased surface area of the photocatalyst during gelation. Optimization or homogenization of the combined materials occurs as the catalyst disperses evenly throughout the gel, creating a uniform surface area, particle size, and distribution. In turn, increasing surface area enhances the efficiency and effectiveness of catalysis because of the homogeneous structure created [33,34]. Recent advancements in sol-gel synthesis processes indicate that controlling the molar ratio of water-to-surfactant may increase the BET surface area by up to 58% [35]. Sol-gel synthesis is cost-effective, requires low energy consumption, and has the potential to produce zero waste during production [36]. When considering synthesizing photocatalysts for water and wastewater treatment, the xerogel method is most commonly used to develop catalysts to obtain nanoparticles for use in part with slurry reactors [37]. While using a slurry method optimizes the surface area of reactive sites available during treatment, the systems require a secondary or membrane filtration to retrieve the photocatalyst and ensure nanoparticles are not introduced to the environment as contaminants [38]. Others have developed silica-based adsorbents designed to filter out organic contaminants at high concentrations [39,40].

Research herein describes an innovative, photocatalytic sol-gel matrix technology that creates a stabilized porous granular media through the utilization of sodium hydroxide, a known foaming agent [41], during solvent extraction. Sodium hydroxide pore infiltration followed by subsequent foaming during firing, aids in retention of the sol-gel networked structure. The resultant material is a very light-weight, highly porous, photocatalytic granular media which can be used as a packed-bed or column treatment systems. Granular media provides for a continuous treatment of contaminated solutions without requiring secondary filtration to recapture the activate treatment agent or photocatalyst. In addition, the porous, absorbent structure of this media creates micro and meso pore spaces that can be leveraged to further treat solution using an electrophilic or nucleophilic attack without need for separate injection. When both photocatalytic and electrophilic or nucleophilic means for treatment are combined, dual treatment can be passively accomplished by

engineering the pore structure and diffusive rate of the electrophile or nucleophile. Further, this pore space can be utilized to passively diffuse buffer solutions for waste streams which require specific pH ranges for optimal treatment to occur. The research presented below demonstrates the reproducibility of the granular structured media, validates the destructive capabilities of the media with bench scale photoreactors, and further defines the long-term sustainability of the media during continuous treatment.

## 2. Results and Discussion

Four concentrations of silicic acid underwent experimentation in order to determine process optimization, SGM product durability, and photocatalytic capabilities (Figure 1). Process characterization and discrete particle testing were performed using thermal gravimetric analysis, forensic inspection using scanning electron microscopy and mercury intrusion porosimetry. The results of particle and/or process characterization are separated below from the corresponding photocatalytic capabilities as the physical engineered characteristics dictate the photocatalytic nature of the SGM.

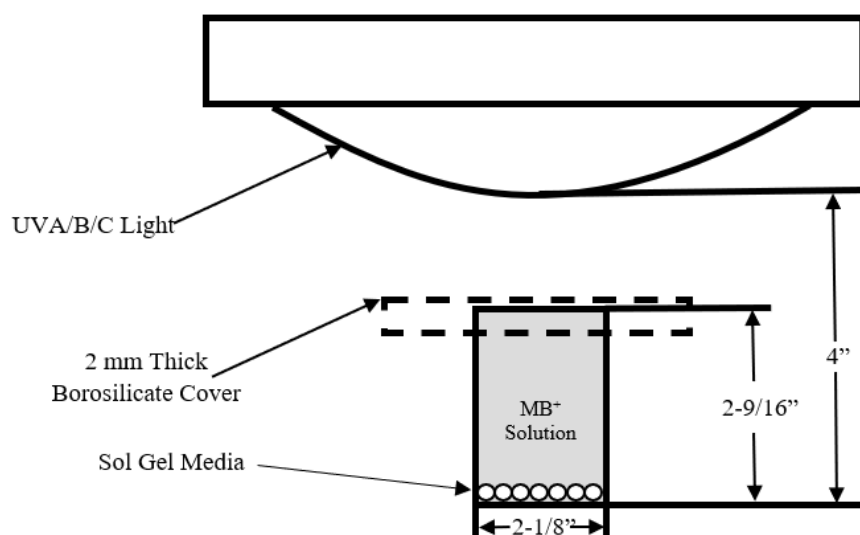


**Figure 1.** Photocatalytic Testing Setup Adapted from ISO 10678.

### 2.1. Photocatalytic Porous Silica-Based Granular Media Characterization

In order to determine the thermal stability of the SGM before and after firing, as well as to measure the mass fraction of volatile components present in the pre and post fired SGM, thermal gravimetric analysis (TGA) was performed. TGA was used to evaluate both the SGM during the gel phase, after being soaked in NaOH, and after complete synthesis of the SGM, post firing. Figure 2 depicts the thermal stability of the SGM as the mass evaluated underwent the firing process described above as compared to the gel phase. A 52% mass loss was recorded during the SGM firing process which directly corresponds to the evaporation of the solvent, or liquid phase, at increasing temperatures. When the gel media is compared to the fired SGM using TGA, very little mass loss is observed, approximately 2%. Minimal mass loss indicates that the pore volume is retained by the foaming agent introduction, supporting the hypothesis that the sodium hydroxide effectively replaces the solvent after 12 h. Additionally, TGA analysis reveals that SGM is stable after firing over a range of temperatures and therefore capable of performing treatment over this range. SGM voids that formed during the gelation process are very clearly demonstrated to be preserved due to the foaming agent, yet the pore volume, structure, and distribution cannot be evaluated using TGA. If these pore structures are to be utilized as a means for additional treatment agents such as a nucleophile or electrophile, characteristics of the pore space distribution, volume, and gradation with respect to the variables of firing temperature and silicic concentration must be evaluated.

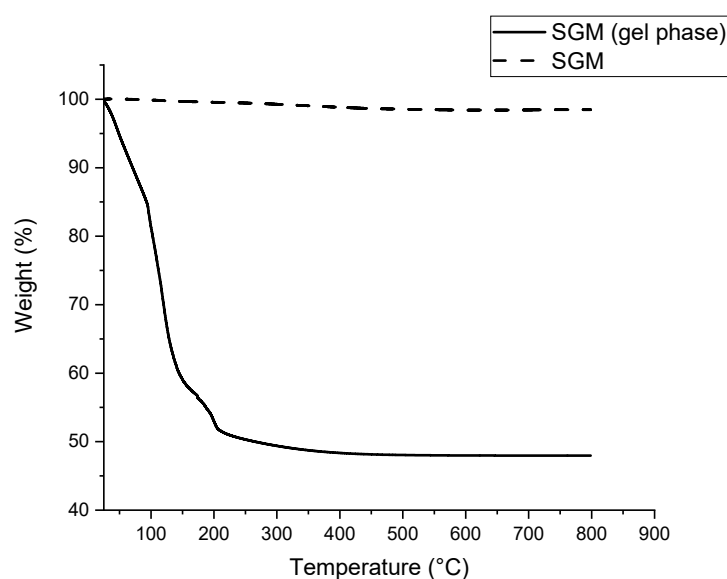


**Figure 2.** Thermal Gravimetric Analysis on Percent Weight loss of SGM during firing.

In order to evaluate the effects of the variables of increasing firing temperature and silica concentrations, visual verification of the pore space post firing was needed. Representative SGM samples randomly selected from each batch were preserved, broken to expose the internal pore space and then prepared for SEM analysis by mounting the samples onto carbon tape. Each sample was examined for pore space using a width of field view from 10 to 12 mm (noted as WD in Figure 3) in backscatter mode and then further evaluated for elemental composition using the electron dispersive spectroscopy (EDS) function. Figure 3 depicts the cross-sectional view of the sample SGM pieces as silicic acid concentrations increased from 5, 50, 500, to 1000 mg/L. Upon visual inspection two distinct forms of void structures are present within the distribution across the cross section. Large void spaces formed during the rapid evaporation and activation of the foaming agent during firing are more readily observed in the SGM containing lower concentrations of silicon. Foaming agent induced pores decrease in abundance and relative size as function of increasing silica in the SGM. This decrease in degassing related pores indicates that the cross-linked polymers are stronger and more durable as silica content increases. There is a background distribution of micro to meso scale pore spaces formed during the cross-linking of the polymer structure. Polymer cross-linked structure preservation, uniformity, and homogeneous size distribution all appear to be directly correlated to increasing silica content within the SGM (the void in the bottom left corner of Figure 3D is a hole in the SGM and is not representative of the SGM structure). An important yet more subtle feature which also corresponds to increasing silica content is the increase in the tortuosity and permeability of the pore space. While the cross-link formed pore-spaces appear smaller in average size, they also appear more interconnected, homogenous in distribution, and uniform in size. An increase in cross-linked structures and decrease in degassing voids can be observed as silicic acid concentrations increase. The increase in cross-linked structures is caused by the increase in nucleation sites the silicic acid brings, thus creating a more durable SGM. Increases in durability and strength of the SGM are demonstrated to improve as the degassing void space decreases and silicic acid concentrations during gelation increase. While structural and thermal strengths have been assessed, the purpose of the SGM is to function as a photocatalytic granular media for water treatment.

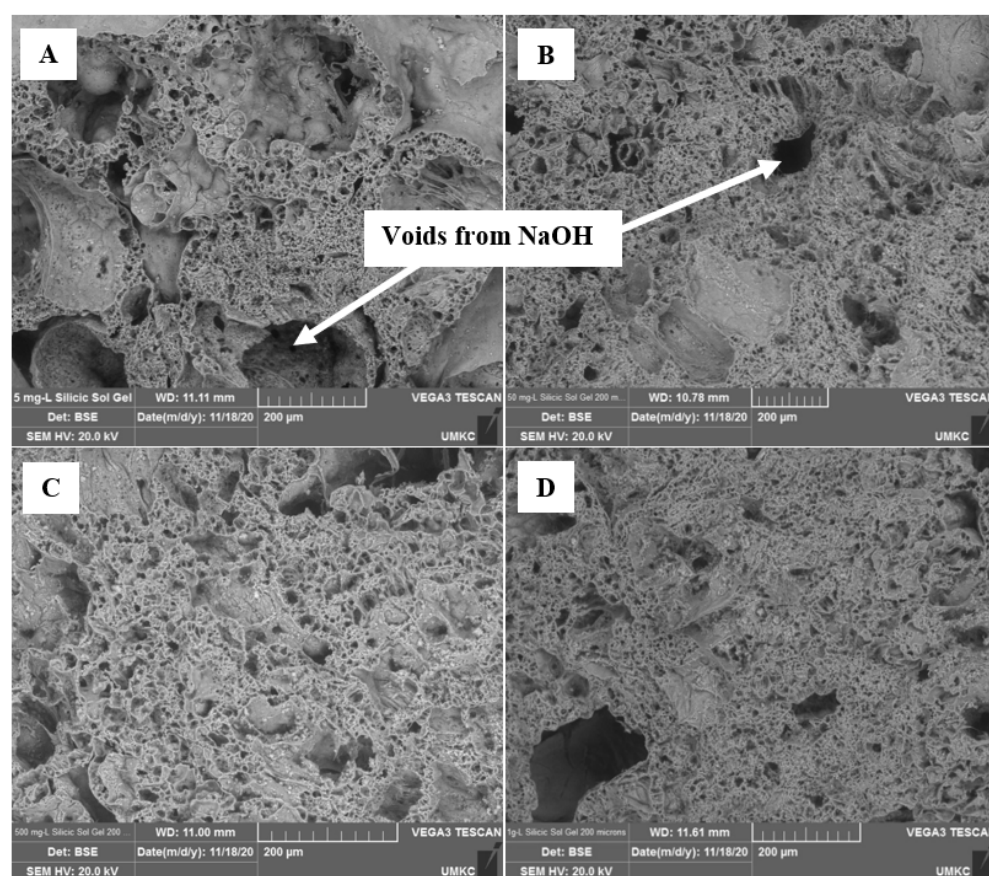


**Figure 3.** SEM Images of (A) 5 mg/L Silicic Acid SGM (B) 50 mg/L Silicic Acid SGM (C) 500 mg/L Silicic Acid and (D) 1000 mg/L Silicic Acid.

A diffusion pore space capable of storing an absorbed solution is observed in the cross-section of SGMs in Figure 3. In order to determine the capacity of the SGM, absorption testing was performed on the various SGM in accordance with ASTM C128 [42]. The test was modified to have an extended saturation period of 72 h due to the presence of significantly more void space relative to traditional aggregates. No other deviations from the standard occurred. The percent absorption was found to be between 50% and 65%, depending on the variation. It is important to note that absorption was observed to decrease with the increase of silicic acid which corresponds to the larger voids formed during off-gassing of foaming agents. Desorption or diffusion of solution from the pore space is dictated by the formation of a thin crust that formed during the firing process. One way to measure the crust thickness or internal to external interface is through mercury intrusion porosimetry (MIP) which evaluates porosity, pore size distribution, and pore volume by intruding mercury into pore space under pressure. At low pressure, the large pore spaces are filled. As pressure increases, mercury is forced into the smaller pores. This process is governed by the Washburn equation which describes the pore aperture as a function of pressure using the non-wetting liquid physical properties. Table 1 presents the results of the MIP analysis performed on four samples representing increasing silica contents.



**Table 1.** Pore Distribution Characteristics and Properties.

	5 mg/L	50 mg/L	500 mg/L	1000 mg/L
<b>Intrusion Data Summary</b>				
Total Intrusion Volume (mL/g)	0.9984	0.8768	1.2206	1.0791
Total Pore Area (m/g)	33.152	34.260	34.450	38.723
Median Pore Diameter (Volume, nm)	750.9	1162.6	1249.6	1014.0
Median Pore Diameter (Area, nm <sup>2</sup> )	17.4	14.9	16.3	16.0
Average Pore Diameter (4 V/A, nm)	120.5	102.4	141.7	111.5
Bulk Density at 0.20 psia (g/mL)	0.5349	0.5981	0.4767	0.4998
Apparent (skeletal) Density (g/mL)	1.1478	1.2576	1.1399	1.0849
Porosity (%)	53.4006	52.4428	58.1829	53.9323
Stem Volume Used (%)	57	46	61	59
<b>Pore Structure Summary</b>				
<b>BET Surface Area (m<sup>2</sup>/g)</b>	162.3000	133.9600	129.2300	156.9500
Tortuosity factor	0.032	0.065	0.044	0.032
Tortuosity	0.9166	1.3234	1.1439	1.2185
<b>Mayer Stowe Summary</b>				
Interstitial porosity (%)	35.0388	36.3433	28.8441	25.9500

It is clear from the MIP pore structure analysis that increasing amounts of silica up to 500 mg/L created a more uniform pore structure, overall porosity, and average pore diameter and volume. Increasing silica higher, to 1000 mg/L, did not produce a more desirable pore structure or overall porosity. Within the 500 mg/L silica SGM, a well graded distribution of pore space is noted, as the average and median pore diameter and volume are both greater than any other variation. BET surface area is a measure of catalyst surface area available to react with a gas or solution. BET surface areas are approximately 33–40% higher than rare titanium dioxide surface area. In addition to pore structure and characterization, the distribution of the pores was compared to differential pressure of intrusion agent. Pore size distribution is calculated with the assumption that the pores are spherical and that larger pore spaces fill with the non-wetting liquid intrusive agent at lower differential pressures, and smaller pores require significantly higher pressure to fill. The distribution curve of pores for the 500 mg/L SGM is presented in Figure 4. Pore distribution is bimodal in that there are large pore spaces that are homogenous in shape and size, while the majority of pore spaces are much smaller with an average size of 80 nm. The bimodal distribution also indicates that there is a 30–40 nm thickness of very dense layer surrounding the smaller pores which is noted in Figure 4 as the curve transitions from horizontal to vertical. All four SGM concentrations examined depicted the same bimodal distribution with the same pore size distribution transition. A working hypothesis is that the crust or shell layer separating the larger pores from the smaller pores is formed as the foaming agent degasses during firing. The exterior of all SGM variations is smooth with no obvious openings, providing some validation of this theory. In addition, the absorption and desorption of solution from the pore space indicates a bimodal trend with larger pores sorbing and desorbing solution faster than smaller pores. The rate at which desorption occurs mimics the pore distribution curve in Figure 4, both of which describe a thin film behavior. The thin shell may function as a control on diffusion of solution from within the microporous structure to solution surrounding the exterior of the media.

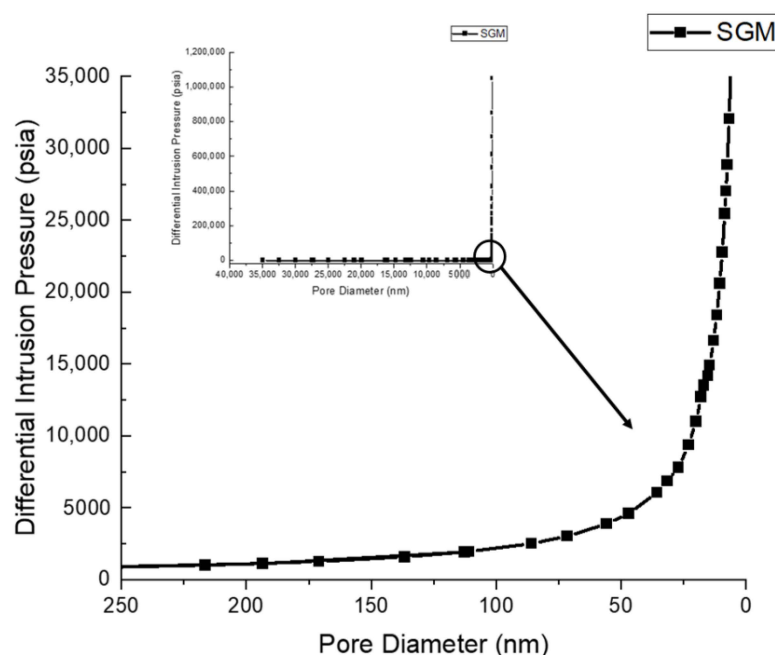


**Figure 4.** Mercury intrusion porosimetry pore size distribution.

Since the SGM was developed as a granular photocatalytic material, understanding the amount and phase of semi-conductor metal used in the media is extremely important. In order to evaluate the source and final photocatalysts, powdered x-ray diffraction (XRD) was performed to determine the major composition of the source. XRD analysis revealed that calcination of the semiconductor metals may have occurred during the firing stage. While both anatase and rutile phases are still present, the intensity of the rutile peaks significantly decreased after the SGM synthesis media process.

## 2.2. Photocatalytic Degradation of Methylene Blue

### 2.2.1. Degradation Kinetics

Photocatalytic reactivity testing was performed on all four variations of SGM utilizing the ISO methodology described in 3.1 (Figure 1). SGM was adhered to the batch reactor to prevent flotation and to ensure that each reactor maintained the same exposed surface area. SGM granules were prewetted to saturated surface dry condition prior to testing. Sample aliquots for each silica concentration SGM were taken every ten minutes from 0 to 60 min as shown in Figure 5. A control was run with no light to validate the degradation of the dye versus adsorption to the SGM. Figure 4 depicts some minimal observed adsorption occurs from 0 to 30 min as the dye wets the surface and the pore space fills, however, there is no change from 30 to 60 min. The primary mechanism for methylene blue reductions by SGM is therefore photolysis, when the dark control data is compared to the data presented in Figure 5. While similar degradation percentages were obtained from all treated SGM variations at 60 min, the 500 mg/L silicic acid SGM had the quickest path to degradation and resulted in 90.6% removal, while the majority of removal (84.6%) removal was achieved after 40 min. The rate of reduction clearly slows down in all reactors as time approaches the hour mark.

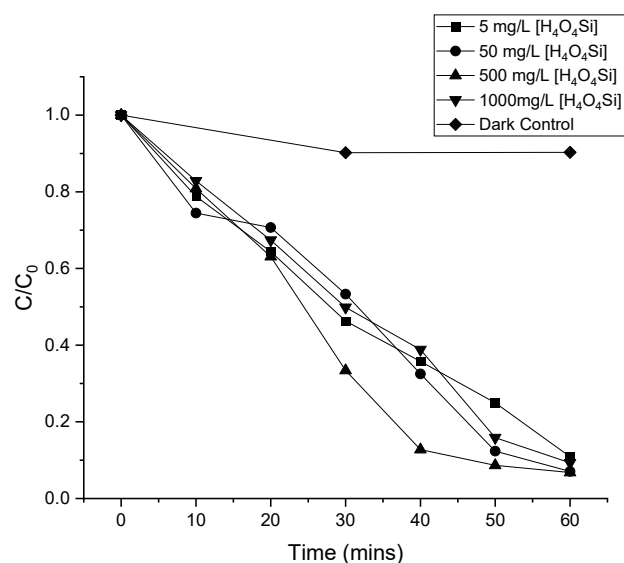


**Figure 5.** Percent Photocatalytic Degradation of Methylene Blue Over Various SGM.

Photocatalytic degradation of methylene blue in SGM is shown to follow first-order degradation kinetics (Figure 5). Figure 6 depicts the linear trend when timed discrete aliquots are plotted against  $\ln(C_0/C)$ . The variance from the fitted line is theorized to be from minimal evaporation of the dye during treatment causing some concentration or from pH influence, as discussed later. Table 2 gives the regression equations and rate constants for the various SGM where the r-squared value is approaching 1 indicating a first-order reaction.

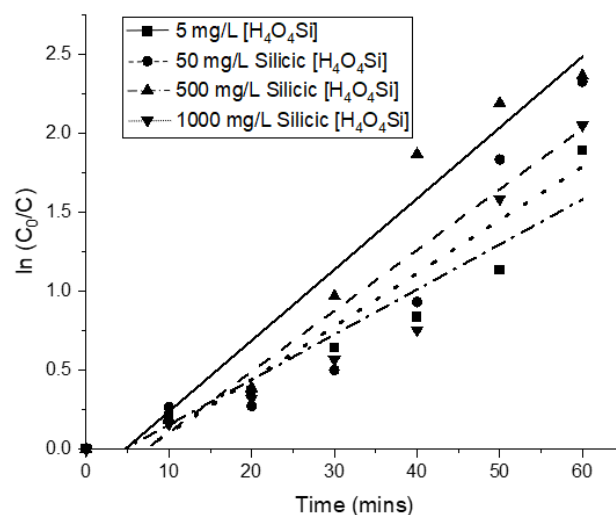


**Figure 6.** Reaction Kinetics of Methylene Blue Over Various SGM

**Table 2.** Regression Equations and Apparent First-Order Rate Constants for Degradation Kinetics of Methylene Blue Over Various SGM.

Silicic Concentration of SGM (mg/L)	$\ln(C_0/C) = kt + b$	$R^2$	$k$ ( $\text{min}^{-1}$ )
5	$\ln(C_0/C) = 0.0286t - 0.131$	0.924	0.0286
50	$\ln(C_0/C) = 0.0385t - 0.278$	0.8882	0.0385
500	$\ln(C_0/C) = 0.045t - 0.2114$	0.9522	0.045
1000	$\ln(C_0/C) = 0.0337t - 0.2342$	0.9054	0.0337



### 2.2.2. Effect of pH on Degradation Kinetics

Literature states the initial pH of MB<sup>+</sup> is between 5.0 and 8.0 S/U, when water is used as a solvent [43]. For this study, the initial MB<sup>+</sup> pH was 6.55. The pH was measured with an Accumet gel-filled electrode calibrated with a standard pH 4.0, 7.0, and 10.0 curve. Measurements of pH occurred over various time increments, in 10 minutes intervals for the entire hour of photostimulated treatment. Figure 7 shows an increase in pH over time and with degradation of MB<sup>+</sup>. This trend opposes general photocatalyzed reactions, considering the byproducts of MB<sup>+</sup> destruction are acidic compounds [43]. The increase in pH is assumed to be diffused excess sodium hydroxide from within the SGM. In order to support this hypothesis, diffusion testing was performed using a 10 to 1 ratio of DI water to SGM. The test was performed on the 500 mg/L silicic acid SGM considering it was the most reactive and all variations followed a similar trend. Figure 8 shows that the pH of a solution increases during continuous contact time with the SGM until equilibrium is reached at about one hour. The extent of this influence is unknown considering no change to the ending pH was observed during cycle testing. Methylene blue degradation is shown to increase with basicity; therefore, the degradations kinetics could be impacted by the increase in pH.

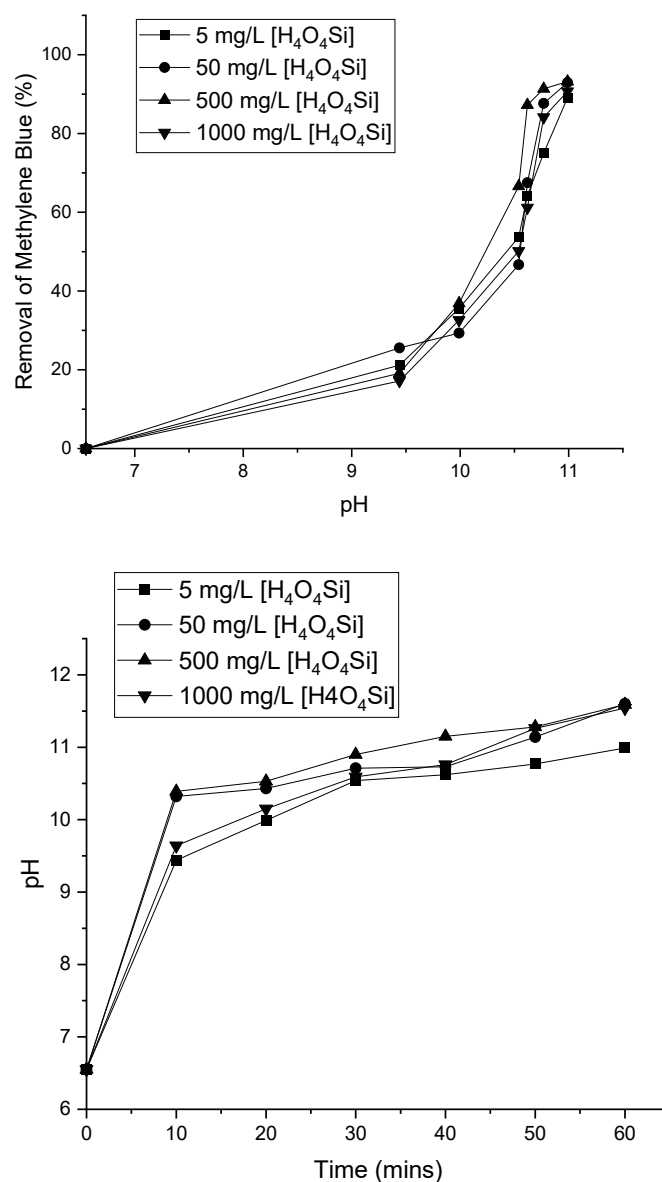
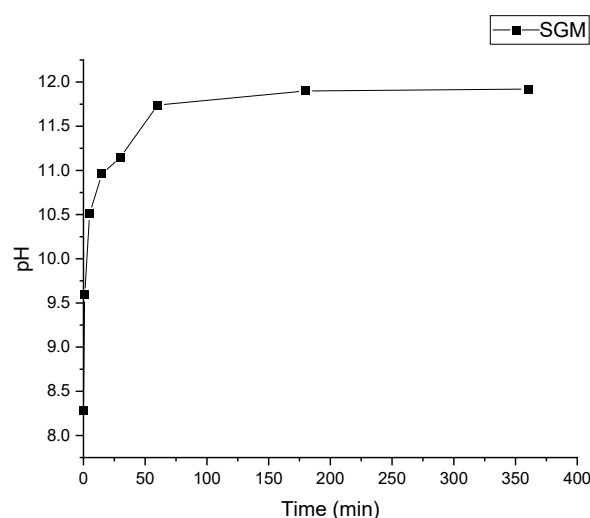
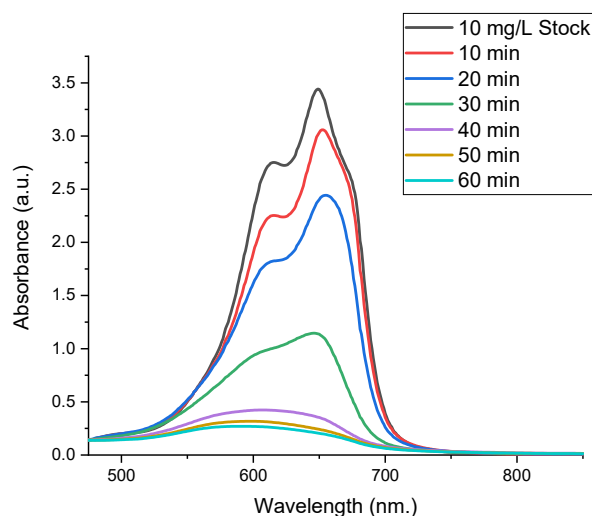


Figure 7. pH of Methylene Blue Over Various SGM.



**Figure 8.** SGM Influence on pH.

While full wavelength spectra analysis was performed on every sample. The 500 mg/L silicic acid SGM is depicted in Figure 9 because it was proven to be the most reactive. Here it can be more easily observed that the degradation percentage is the greatest between 20 and 30 min. Similarly, the greatest increase in pH was found to be from 20 to 30 min, further validating the influence of pH on degradation kinetics.



**Figure 9.** Methylene Blue Degradation by 500 mg/L Silicic SGM.

### 2.2.3. Sustained Photocatalytic Reactivity with Added Amendments to the SGM

The variations of SGM were further tested in a cyclic form with additions of de-ionized water ( $\text{H}_2\text{O}$ -SGM), nitric acid ( $\text{HNO}_3$ -SGM), and sodium thiosulfate ( $\text{Na}_2\text{S}_2\text{O}_3$ -SGM) to the pore space. SGM media were adhered to the reactor, filled with  $\text{MB}^+$  solution, tested, the solution decanted from the reactor, and then refilled for another reactor test cycle. SGM without anything loaded in the pore space was tested as a control for comparison of performance. For this study, the amendments were preloaded into the pore space by soaking the SGM in a one molar concentration of their respective solutions for 72 h. Vacuum impregnation could be used as an alternative to soaking to ensure that all pores are preloaded with the diffusive solution of choice. Cycles were performed in 45-min allotments and recycled a total of four times (Figure 10).

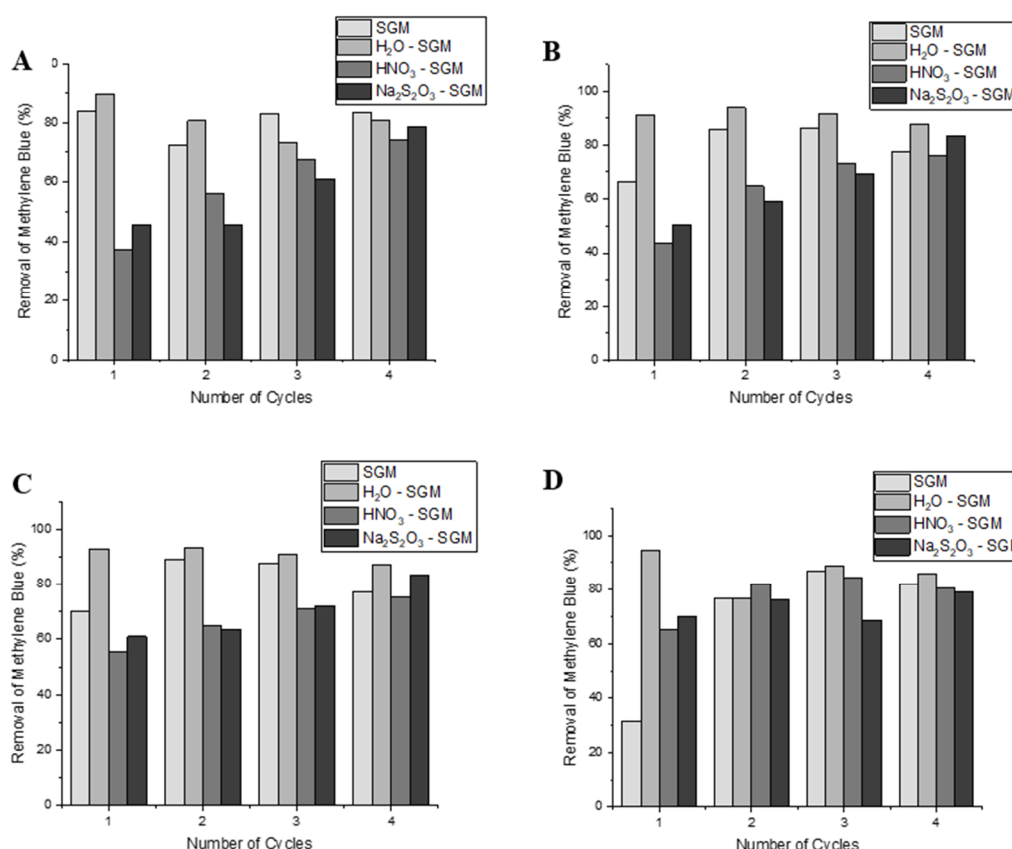


**Figure 10.** Photocatalytic Cyclic Testing over (A) 5 mg/L Silicic Acid SGM (B) 50 mg/L Silicic Acid SGM (C) 500 mg/L Silicic Acid and (D) 1000 mg/L Silicic Acid, with various amendments.

The stability and reactivity of the SGM were analyzed by the removal of MB<sup>+</sup> and the visual appearance of the media over each cycle. For cycle 1, the unsoaked granule noted in Figure 10 as “SGM” was found to decrease in MB<sup>+</sup> treatment removal as the content of silicic acid concentrations increased (Figure 10 A–D). Increasing silica appears to inhibit the ability for the dye to adsorb onto the surface of the photocatalyst as increasing silica within the SGM encapsulates the titanium dioxide. Considering the short lifespan of reactive radicals, they are normally diffused to the photocatalytic surface and react with the adsorbed molecules. Therefore, the longer it takes for the contaminant to adsorb to the surface, the longer it will take to remove the compound. This phenomenon is only observed in cycle 1 of all “SGM” labelled batches across all four concentrations, as the surface and pore space were wetted in subsequent cycles the performance was comparable to the other treatments.

The addition of both nitric acid and sodium thiosulfate treatments hindered the removal efficiency for MB<sup>+</sup> for all concentrations but is most pronounced in the SGM batches corresponding to higher absorption capacities (5 and 50 mg/L silicic acid). However, the addition of nitric acid has the ability to act as an internal pH buffer in acidic conditions (Figure 11). Future uses of the internal pore space could include various treatments which diffuse from the microstructure of internal pores, through the thin shell of the SGM, and then contribute to the overall wetting solution. In these situations, the desired acid and concentration to preload into the SGM would be determined by the compounds of concern in the waste stream and optimal final pH for degradation. Cyclic testing verified the ability of the SGM to buffer the solution to a pH equivalent to the equilibrium of the media, which was determined to be just under pH 12.0 during diffusion testing. The stability and durability of the SGM becomes a concern when the pH of solution exceeds the natural pH of the media. Of primary concern is cleaving of silica–oxygen–silica bonds at pH elevated above 12.0. Therefore, no addition treatment agents can be incorporated within the pore

space that will increase the pH greater than 12 for a sustained amount of time. The pH of the SGM with no additional treatments and DI water addition were statistically indifferent, therefore, only one was reported. The sodium thiosulfate incorporated within the pore space had no influence on the pH.

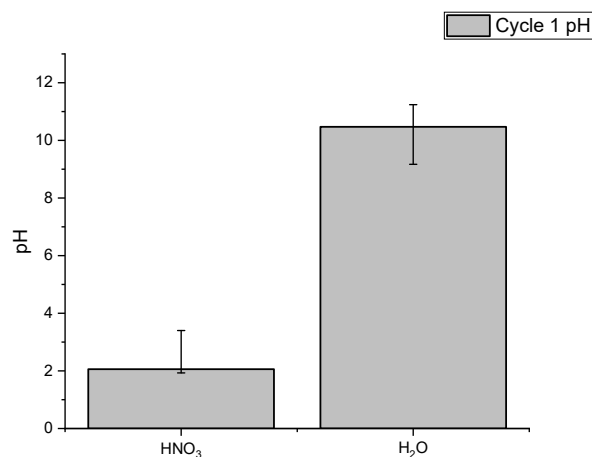


**Figure 11.** pH of Methylene Blue After One Cycle.

The longevity of the SGM was tested over four continuous cycles. General trends showed the DI water soaked SGM consistently performed better at all variations of the media. While there was some variance in the removal of MB<sup>+</sup> over cycles, the percent removed stayed between +/−10%. The 50 mg/L and 500 mg/L were the most consistent SGMs, with removal only varying between +/−5%. Further testing was performed on these SGM variations to determine the optimal mixture design for the removal of methylene blue.

#### 2.2.4. Determination of the Most Efficient SGM

Cyclic testing was performed for six cycles over both the 50 mg/L and 500 mg/L SGM to determine which SGM was most effective in the continuous removal of MB<sup>+</sup>. The SGM was soaked in DI water for 24 h prior to testing and then dried to saturated surface dry condition. The SGM was tested utilizing both 10 mg/L and 20 mg/L methylene blue to test the reactivity at higher contaminant concentrations (Figure 12). Cycles were performed in 60-min allotments and continuously recycled.

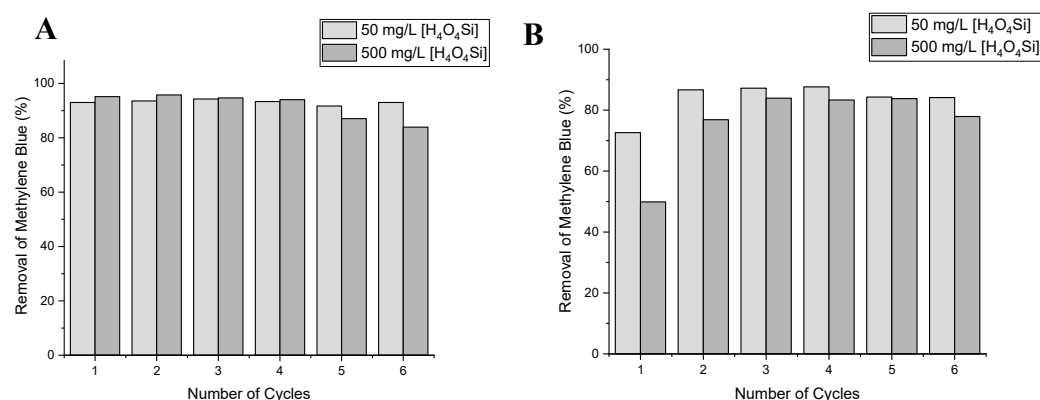


**Figure 12.** (A) 10 mg/L Methylene Blue Degradation by SGM (B) 20 mg/L Methylene Blue Degradation by SGM.

Advantages and disadvantages of both SGM variations were observed during cyclic testing. For the 10 mg/L MB<sup>+</sup>, maximum removal was 94.29% for the 50 mg/L silicic acid SGM (50-SGM) and 95.79% for the 500 mg/L silicic acid SGM (500-SGM). While the

50-SGM varied less than 2% over cycles with continuous removal over 90%, the 500-SGM varied just over 10%. The 20 mg/L MB<sup>+</sup> had a maximum removal of 87.65% for the 50-SGM and 83.83% for the 500-SGM. The first cycle had a significantly lower removal percentage which is assumed to be a delay in the adsorption of the dye to the photocatalyst to begin degradation.

While the absorbance of MB<sup>+</sup> over cycles was used to determine efficiency of the SGM, visual observations were also made. Solids appeared in the solution of the 50-SGM in the 4th cycle but did not seem to have a large influence on the absorbance of the MB<sup>+</sup>. No solids were visible in the 500-SGM. This observation notes that the stability of the structure of the SGM increases with silicic acid concentration.

The photocatalytic reactivity of both the 50-SGM and 500-SGM show continuous removal capacity of methylene blue. The 50-SGM shows a higher efficiency of removal in both concentrations of MB<sup>+</sup> by the sixth cycle. However, the durability and stability of the 50-SGM significantly lessens overtime, therefore, the 500-SGM is determined to be the most suitable SGM for continuous treatment of methylene blue.

#### 2.2.5. SGM Condition after Cyclic Testing

After cyclic testing was completed, forensic analysis was carried out on the SGM to determine the condition of the photocatalyst. Figure 13 shows the distribution of the silicon and titanium within the SGM in SEM-EDS at microscale. In the image areas colored red are titanium, while those colored blue are silicon. In SEM-EDS imagery the darker and more intense the color, the higher the concentration of that element. While there are some places with either one of the elements is more predominant, it can be observed that the photocatalyst is homogeneously immobilized within the media and does not appear to leach out over time. Fixating the photocatalyst within the SGM is one priority factor that allows SGM to continuously perform treatment without the need for secondary filtration unlike slurry treatment techniques.

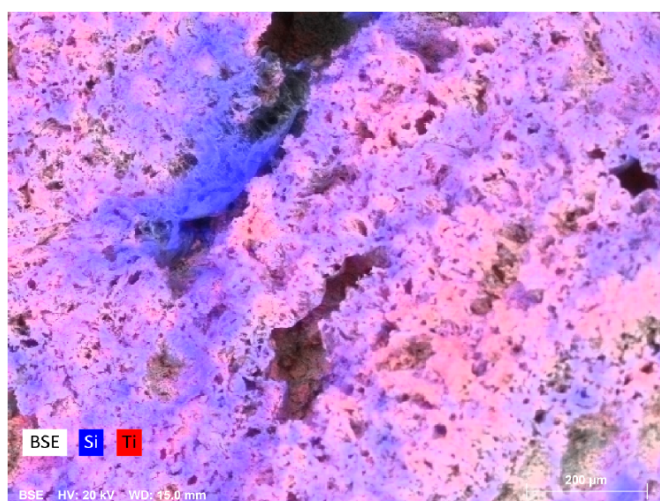


**Figure 13.** SEM/EDS Image of SGM after Cyclic Testing.

While fixation of the photocatalyst is an important aspect of SGM, it is still possible for a fixated photocatalyst to convert to other forms or the ratio of anatase to rutile may change. XRD analysis was performed on the SGM before and after cycle testing (Figure 14). The titanium dioxide (P25) used in synthesis of the SGM was analyzed for comparison of the anatase and rutile peaks. While the intensities of the peaks were suppressed by the silica content in the SGM, it is apparent that the peaks do not shift or broaden in the anatase and rutile peaks noted. Also, no notable changes were exhibited in the SGM patterns before and after cyclic testing, showing no alterations to the SGM occur during testing.



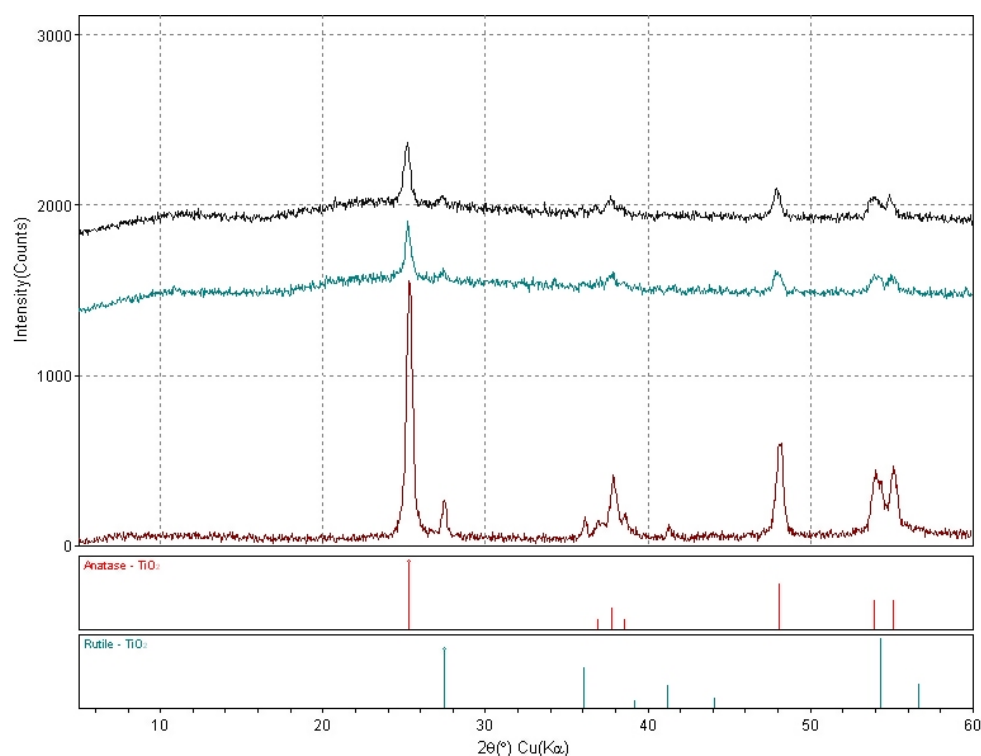


**Figure 14.** XRD Pattern of SGM Before and After Cyclic Testing Compare to the  $\text{TiO}_2$  Photocatalyst Used.

### 3. Experimental Methods and Materials

#### 3.1. Materials

Materials utilized to create the stabilized sol-gel structure and used in photocatalytic testing include the alkoxide precursors, acid and base catalysts, photocatalysts, foaming agents, electrophiles, and nucleophiles. Tetraethyl orthosilicate (TEOS), tetramethyl orthosilicate (TMOS), titanium (IV) oxide, Aeroxide<sup>®</sup> P25, ACROS Organics, and nitric acid were purchased from Thermo Fisher Scientific (Waltham, MA, USA) with lot numbers A0420038, A0408640, A0407014, and 147594, respectfully. Sodium hydroxide (B1750262), potassium hydroxide (B1558512), and silicic acid (B0148079) were purchased from Sigma Aldrich (St. Louis, MO, USA). Reagent grade sodium thiosulfate, acetic acid, and hydrochloric acid were used. In order to determine the long-term sustainability of the media over time, initial X-ray diffraction (XRD) analysis of the titanium dioxide ( $\text{TiO}_2$ ) was performed and yielded a composition primarily composed of anatase with minor rutile.

#### 3.2. Photocatalytic Porous Silica-Based Granular Media Development

The overarching goal of this research was to develop a porous, photocatalytic, granular media to be utilized in a packed column or bed, for passive, continuous treatment of organic contaminants in solution. Optimal combinations of precursor to water mixtures were performed in bench scale testing using an iterative, partial factorial approach that controlled for concentration, ratio, and process. In order to determine the most favorable conditions and processes, photocatalytic porous silica-based media (SGM) synthesis was conducted with various precursors, acid catalysts, base catalysts, material ratios, temperature, and solvent extraction processes to determine a suitable media for continuous treatment of methylene blue.

While both tetraethyl orthosilicate and tetramethyl orthosilicate were examined as viable precursors for structural stability of SGM, TEOS is the more cost effective and industrializable precursor for SGM applications. The addition of acid and base catalysts was used to control the time to gelation and ultimate a porous structure. Acetic acid,

hydrochloric acid, silicic acid, nitric acid, sodium hydroxide, and potassium hydroxide were examined in a testing matrix of concentration and volume over various TEOS to water ratios. While all of the examined acids and bases listed were suitable for developing a sol-gel, strong acid and bases heavily favored the irreversible forward reaction hence creating a very weak cross-linked structure. Silicic acid the most appropriate catalyst as silica acts as a nucleation site during polymerization as well as possessing the ability to lower the solution pH sufficiently to promote hydrolysis without introducing leachable compounds to the SGM. In addition, since silicic acid is a weak acid, gelation was readily controllable during heating.

Aerogels are ultralight, porous materials in which collapse of the gel network is prevented by replacement of solvent by gas. Solvent extraction to develop a porous media include supercritical drying, ambient pressure with matrix strengthening, or freeze-drying methods, leading to the synthesis of an aerogel [44,45]. Of these three methods, supercritical drying is the most commonly utilized variation of aerogel solvent extraction. Supercritical drying requires special pressure vessel capable of high pressure, in which supercritical carbon dioxide is continuously passed over the gel to extract the solvent. Super critical drying requires specialized equipment, skilled technicians, and potentially harmful gas to reproducibly synthesize aerogels. With the introduction of a foaming agent into the solvent system, described below, supercritical conditions were bypassed as unnecessary. While various foaming agents or hydroxides were tested for maximum pore structure retention with minimum loss of material, sodium hydroxide yielded the best results. Sodium hydroxide was introduced to the sol-gel in gelation phase prior to firing at various concentrations in order to determine optimized conditions. This step proved to be crucial to the sol gel media process as higher concentrations of NaOH cleave the Si–O–Si bonds that make up the gel network [46] and result in the dissolution of the gel. However, too low of a sodium hydroxide concentration over short lengths of exposure did not fully allow for foaming agent penetration, resulting in the gel forming powder upon firing. Once optimal concentrations and immersion times were determined for sodium hydroxide, the media was placed on a ceramic sheet and fired. Various activation temperatures were utilized in order to optimize the foaming agent's release from the pore solutions and therefore produce the most homogenous and well distributed pore structure. Note that the foaming agent is not activated at ambient conditions and requires some heat to retain the 3D cross-linked network. A temperature over 300 °C was required for activation of the foaming agent, however, above 450 °C the titanium photocatalyst converted to predominantly rutile.

Once the general process for SGM was devised, further testing for the optimal mixture proportions was performed. Initial SGM synthesis and photocatalytic testing indicated the optimal silica to titania ratio for structural stability and reactivity was approximately a 4:1 (SiO<sub>2</sub>:TiO<sub>2</sub>) ratio. Addition of titanium dioxide exceeding this ratio produced a powder upon firing, rather than a porous media. Silica in excess of the 4:1 ratio inhibited or shielded the photocatalyst within the media or on the surface, causing the media to be less photocatalytically active. Trends showed durability of the SGM structure increased with an increasing concentration of silicic acid up to an optimized point before reactivity began to decrease due to armoring of photocatalyst discussed above. This study further investigates the extents of this trend to determine the optimal SGM mixture for continuous cyclic batch testing of the photocatalytic removal of methylene blue.

### 3.3. Photocatalytic Porous Silica-Based Granular Media Synthesis

Media synthesis was performed following a hydrolysis/condensation reaction mechanism [47] and utilizing TEOS as a precursor, silicic acid as a catalyst, and TiO<sub>2</sub> as a photocatalyst. During this process, 9 g of TiO<sub>2</sub> was dissolved in 150 mL of TEOS and 150 mL of silicic acid at various concentrations (5, 50, 500, and 1000 mg/L). The solution was stirred at 55 °C until gelation was complete, approximately 12 h after initial mixing. The gelled sample was then broken into the desired size or gradation for the testing protocol needed, e.g., column or batch reactors. For this study spherical pieces about 1 cm

in diameter were created in order to match the reactor vessel. Pieces of the broken gel were placed into 1M NaOH for a minimum of 12 h to allow for the foaming agent to displace solvent within pore space. However, with the chosen concentration, less than 2% of the gel mass was lost during the soaking process. Once the gel was fully saturated with the foaming agent (NaOH), the gel was fired at 400 °C. Four variations of SGM at increasing concentrations of silica were chosen for further analysis and photocatalytic efficiency testing. In addition, forensic investigation of the structure and durability of the SGM was performed using scanning electron microscopy (SEM) (UMKC) imaging and mercury intrusion porosimetry (MIP) (Tuscon, AZ, USA) to analyze the porosity and pore distribution.

### 3.4. Photocatalytic Testing

A modified testing procedure of the photocatalytic reactivity of the SGM was adapted from the International Organization for Standardization standard ISO 10678 [Fine ceramics (advanced ceramics, advanced technical ceramics); Determination of photocatalytic activity of surfaces in an aqueous medium by degradation of methylene blue] [48]. Methylene blue ( $\text{MB}^+$ ) is a common contaminant in textile wastewater [49] and is routinely used as a surrogate to test organic pollutant reduction capacity.  $\text{MB}^+$  degradation highlights the efficiency of photocatalytic degradation capabilities and is considered optimal for lab testing considerations because degradation of the structure results in a drastic color change from dark blue to clear as the progressive destruction of the compound forms  $\text{CO}_2$  and  $\text{H}_2\text{O}$  byproducts [42,50]. Methylene blue possesses a high absorptivity with a maximum absorption occurring at a wavelength between 660 and 665 nm [51,52].

Photocatalytic testing of the SGM was performed using the batch reactor setup shown in Figure 1. 35 mL  $\text{MB}^+$  solution was pipetted to cover a single layer of SGM adhered to the bottom of the batch reactor. SGM weighed approximately 3 grams per batch test, which equates to approximately 0.10 grams of photocatalyst depending upon the concentration of silicic acid under evaluation. UVA/B/C lights operating over a wide range of wavelengths from 550 to 250 nm were precisely placed above the targeted SGM at a height of 4". Experiments involving cycle testing required that the initial solution be discarded and another 35 mL of  $\text{MB}^+$  pipetted onto the SGM which was then immediately placed back under the light. Minimal disturbances of the UV light source interacting with the targeted SGM were attempted and all deviations or movements of SGM, solution, and light interactions were kept at a minimum to insure replicability. Aliquots of solutions were extracted at various time intervals in order to obtain kinetic representation of the degradation potential. In addition, extracted aliquot solutions were cooled in a darkened container prior to further analysis. Concentrations of methylene blue analysis was conducted using a DR3900 Hach UV-Vis Spectrometer (UMKC) and identical matching 10ml quartz cuvettes. Prior to testing, calibration of the methylene blue was performed with  $\text{MB}^+$  concentrations of 0, 10, 20, 30, 40, and 50 mg/L and a linear relationship of absorption to concentration was achieved. Full spectrum analysis indicated 660 nm was the primary peak wavelength for methylene blue examined in this study. Each aliquot sample analysis was performed in triplicate for absorbance at 660 nm, with full wavelength scans performed at least once per sample in order to determine when secondary or degradation peaks were observed.

## 4. Applications and Future Testing

An optimized SGM variation was finalized for a sustained photocatalytic reactivity and therefore treatment for organic contaminants in solution. The 50 mg/L SGM possessed the best treatment of  $\text{MB}^+$  performance, however, variations to the design and treatment of pore space can be performed in order to target a specific waste stream. Amendments were added to the pore space with the intent to slowly diffuse through the thin shell and assist in treatment performance. Treatment within the pore space clearly show the diffusive abilities of the SGM while in contact with the waste stream. While these compounds did not necessarily have a positive impact on the degradation of  $\text{MB}^+$ , diffusion of various

amendments from the pore space provides the additional capacity of the SGM to have either an electrophile or nucleophile attack on the contaminants of concern. Salts are known to decrease the surface tension in perfluoroalkyl acids [53] and can be used to improve removal efficiency of these compounds [54]. The utilization of the porous media introduces the ability to treat numerous contaminants and waste streams, with possibility to treat PFAS bearing waste streams.

Bench scale tests were performed for this study to determine the most feasible SGM as a packed bed or column water treatment system. While the performance of the SGM was established, additional work remains to be done. Future testing will be performed utilizing the media in a packed column (Figure 15). A column system will allow for continuous treatment of the waste stream in a very industrial driven design. SGM is optimal for this type of system as the gradation of the SGM can be controlled for, thus allowing treatment to be performed on the optimized gradation for contact time or reaction rates. Future testing on various organic contaminants, degradation kinetics, and flow rates in order to determine the required contact time and reaction rates.

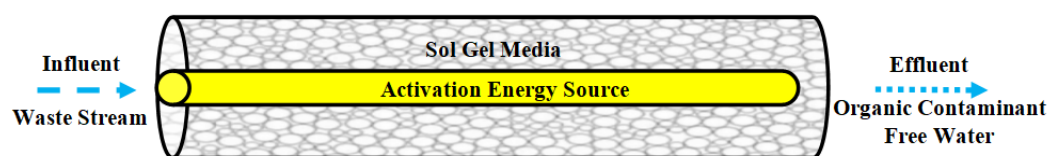


Figure 15. Rapid Testing Column Schematic.

## 5. Conclusions

A photocatalytic porous silica-based granular media was synthesized for continuous photocatalytic degradation of organic contaminants. Methylene blue was utilized as a surrogate contaminant for textile dyes. An initial testing matrix was utilized to determine a general method and process for synthesis of the SGM. The 3D structure of the polymer was retained through addition of a foaming agent, which has previously never been studied as a solvent extraction method. Further testing was performed on various ratios of silica to titania to determine a mixture design for a highly reactive and sustainable SGM. The porous structure allows for introduction of amendments that can be utilized in the degradation of the contaminants or as a pH buffer. The SGM was successful in removing over 90% of methylene blue in one hour and consistently performed at this for capacity in multiple successive cycles. The vast variability control of the SGM design allows for the media to be designed for general treatment purposes or tailored for a specific contaminant. Given the ease and low energy consumption of synthesis, the versatility of application, and continuous reactivity over time, the SGM is a promising media for treatment of organic contaminants in aqueous phase.

**Author Contributions:** Funding acquisition, M.L.H.; Investigation, H.M.M.; Methodology, H.M.M.; Supervision, M.L.H.; Writing—original draft, H.M.M.; Writing—review—editing, M.L.H. Both authors have read and agreed to the published version of the manuscript.

**Funding:** This research was funded by SERDP grant #ER19-1404.

**Acknowledgments:** (<https://www.serd-estcp.org/Program-Areas/Environmental-Restoration/ER19-1403>) (accessed on 14 February 2021). The authors would also like to thank Geosyntec for their assistance. This technology is protected by a provisional patent.

**Conflicts of Interest:** The authors declare no conflict of interest.

## References

1. Lellis, B.; Fávaro-Polonio, C.Z.; Pamphile, J.A.; Polonio, J.C. Effects of textile dyes on health and the environment and bioremediation potential of living organisms. *Biotechnol. Res. Innov.* **2019**, *3*, 275–290. [[CrossRef](#)]
2. Brillas, E.; Martínez-Huitle, C.A. Decontamination of wastewaters containing synthetic organic dyes by electrochemical methods. An updated review. *Appl. Catal. B Environ.* **2015**, *166–167*, 603–643. [[CrossRef](#)]

3. Hassaan, M.A.; El Nemr, A. Health and Environmental Impacts of Dyes: Mini Review. *Am. J. Environ. Sci. Eng.* **2017**, *1*, 64–67. [\[CrossRef\]](#)
4. Raval, N.P.; Shah, P.U.; Shah, N.K. Malachite green “a cationic dye” and its removal from aqueous solution by adsorption. *Appl. Water Sci.* **2017**, *7*, 3407–3445. [\[CrossRef\]](#)
5. Khan, S.; Malik, A. Toxicity evaluation of textile effluents and role of native soil bacterium in biodegradation of a textile dye. *Environ. Sci. Pollut. Res.* **2018**, *25*, 4446–4458. [\[CrossRef\]](#)
6. Hueber-Becker, F.; Nohynek, G.J.; Dufour, E.K.; Meuling, W.J.; De Bie, A.T.; Toutain, H.; Bolt, H.M. Occupational exposure of hairdressers to [14C]-para-phenylenediamine-containing oxidative hair dyes: A mass balance study. *Food Chem. Toxicol.* **2007**, *45*, 160–169. [\[CrossRef\]](#)
7. Cassano, A.; Molinari, R.; Romano, M.; Drioli, E. Treatment of aqueous effluents of the leather industry by membrane processes. *J. Membr. Sci.* **2001**, *181*, 111–126. [\[CrossRef\]](#)
8. Albano, G.; Colli, T.; Nucci, L.; Charaf, R.; Biver, T.; Pucci, A.; Aronica, L.A. Synthesis of new bis[1-(thiophenyl)propynones] as potential organic dyes for colorless luminescent solar concentrators (LSCs). *Dyes Pigment.* **2020**, *174*, 108100. [\[CrossRef\]](#)
9. Samchetshabam, G.; Hussan, A.; Choudhury, T.G. Impact of Textile Dyes Waste on Aquatic Environments and its Treatment Impact of Textile Dyes Waste on Aquatic Environments and its Treatment. *Environ. Ecol.* **2017**, *35*, 2349–2353.
10. Chiu, Y.-H.; Chang, T.-F.M.; Chen, C.-Y.; Sone, M.; Hsu, Y.-J. Mechanistic Insights into Photodegradation of Organic Dyes Using Heterostructure Photocatalysts. *Catalysts* **2019**, *9*, 430. [\[CrossRef\]](#)
11. Katafias, A.; Lipińska, M.; Strutyński, K. Alkaline hydrogen peroxide as a degradation agent of methylene blue—Kinetic and mechanistic studies. *React. Kinet. Mech. Catal.* **2010**, *101*, 251–266. [\[CrossRef\]](#)
12. Aa, O.; Aj, O. Kinetic Study of Decolorization of Methylene Blue with Sodium Sulphite in Aqueous Media: Influence of Transition Metal Ions. *J. Phys. Chem. Biophys.* **2014**, *2*, 1–7. [\[CrossRef\]](#)
13. Ahmed, M.; Abou-Gamra, Z.; Salem, A. Photocatalytic degradation of methylene blue dye over novel spherical mesoporous Cr<sub>2</sub>O<sub>3</sub>/TiO<sub>2</sub> nanoparticles prepared by sol-gel using octadecylamine template. *J. Environ. Chem. Eng.* **2017**, *5*, 4251–4261. [\[CrossRef\]](#)
14. Liu, H.; Guo, W.; Li, Y.; He, S.; He, C. Photocatalytic degradation of sixteen organic dyes by TiO<sub>2</sub>/WO<sub>3</sub>-coated magnetic nanoparticles under simulated visible light and solar light. *J. Environ. Chem. Eng.* **2018**, *6*, 59–67. [\[CrossRef\]](#)
15. Zhu, S.; Wang, D. Photocatalysis: Basic Principles, Diverse Forms of Implementations and Emerging Scientific Opportunities. *Adv. Energy Mater.* **2017**, *7*, 1–24. [\[CrossRef\]](#)
16. Akerdi, A.G.; Bahrami, S.H. Application of heterogeneous nano-semiconductors for photocatalytic advanced oxidation of organic compounds: A review. *J. Environ. Chem. Eng.* **2019**, *7*, 103283. [\[CrossRef\]](#)
17. Fujishima, A.; Honda, K. Electrochemical Photolysis of Water at a Semiconductor Electrode. *Nat. Cell Biol.* **1972**, *238*, 37–38. [\[CrossRef\]](#)
18. Fujishima, A.; Rao, T.N.; Tryk, D.A. Titanium dioxide photocatalysis. *J. Photochem. Photobiol. C Photochem. Rev.* **2000**, *1*, 1–21. [\[CrossRef\]](#)
19. Martha, S.; Sahoo, P.C.; Parida, K.M. An overview on visible light responsive metal oxide based photocatalysts for hydrogen energy production. *RSC Adv.* **2015**, *5*, 61535–61553. [\[CrossRef\]](#)
20. Belachew, N.; Kahsay, M.H.; Tadesse, A.; Basavaiah, K. Green synthesis of reduced graphene oxide grafted Ag/ZnO for photocatalytic abatement of methylene blue and antibacterial activities. *J. Environ. Chem. Eng.* **2020**, *8*, 104106. [\[CrossRef\]](#)
21. Hu, Z.; He, Q.; Ge, M. Photocatalytic degradation of organic contaminants by magnetic Ag<sub>3</sub>PO<sub>4</sub>/MFe<sub>2</sub>O<sub>4</sub> (M = Zn, Ni, Co) composites: A comparative study and a new insight into mechanism. *J. Mater. Sci. Mater. Electron.* **2020**, *4*. [\[CrossRef\]](#)
22. Nuengmatcha, P.; Porrawatkul, P.; Chanthai, S.; Sricharoen, P.; Limchoowong, N.; Sricharoen, P. Enhanced photocatalytic degradation of methylene blue using Fe<sub>2</sub>O<sub>3</sub>/graphene/CuO nanocomposites under visible light. *J. Environ. Chem. Eng.* **2019**, *7*, 103438. [\[CrossRef\]](#)
23. Xu, B.; Ahmed, M.B.; Zhou, J.L.; Altaee, A.; Wu, M.; Xu, G. Photocatalytic removal of perfluoroalkyl substances from water and wastewater: Mechanism, kinetics and controlling factors. *Chemosphere* **2017**, *189*, 717–729. [\[CrossRef\]](#) [\[PubMed\]](#)
24. Dariani, R.; Esmaeili, A.; Mortezaali, A.; Dehghanpour, S. Photocatalytic reaction and degradation of methylene blue on TiO<sub>2</sub> nano-sized particles. *Optik* **2016**, *127*, 7143–7154. [\[CrossRef\]](#)
25. Liu, M.; Yin, W.; Qian, F.-J.; Zhao, T.-L.; Yao, Q.-Z.; Fu, S.-Q.; Zhou, G.-T. A novel synthesis of porous TiO<sub>2</sub> nanotubes and sequential application to dye contaminant removal and Cr(VI) visible light catalytic reduction. *J. Environ. Chem. Eng.* **2020**, *8*, 104061. [\[CrossRef\]](#)
26. Xu, C.; Rangaiah, G.P.; Zhao, X.S. Photocatalytic Degradation of Methylene Blue by Titanium Dioxide: Experimental and Modeling Study. *Ind. Eng. Chem. Res.* **2014**, *53*, 14641–14649. [\[CrossRef\]](#)
27. Grande, F.; Tucci, P. Titanium Dioxide Nanoparticles: A Risk for Human Health? *Mini Rev. Med. Chem.* **2016**, *16*, 762–769. [\[CrossRef\]](#) [\[PubMed\]](#)
28. Pouloupoulos, S.G.; Yerkinova, A.; Ulykbanova, G.; Inglezakis, V.J. Photocatalytic treatment of organic pollutants in a synthetic wastewater using UV light and combinations of TiO<sub>2</sub>, H<sub>2</sub>O<sub>2</sub> and Fe (III). *PLoS ONE* **2019**, *14*, e0216745. [\[CrossRef\]](#)
29. Khadary, N.H.; Alkhouraji, W.S.; Sakthivel, T.S.; Khadary, D.N.; Salam, M.A.; Alshihri, S.; Al-Mayman, S.I.; Seal, S. Synthesis of Superior Visible-Light-Driven Nanophotocatalyst Using High Surface Area TiO<sub>2</sub> Nanoparticles Decorated with Cu<sub>x</sub>O Particles. *Catalysts* **2020**, *10*, 872. [\[CrossRef\]](#)



30. Luttrell, T.; Halpegamage, S.; Tao, J.; Kramer, A.; Sutter, E.A.; Batzill, M. Why is anatase a better photocatalyst than rutile?—Model studies on epitaxial TiO<sub>2</sub> films. *Sci. Rep.* **2015**, *4*, 4043. [CrossRef]
31. Li, R.; Jia, Y.; Bu, N.; Wu, J.; Zhen, Q. Photocatalytic degradation of methyl blue using Fe<sub>2</sub>O<sub>3</sub>/TiO<sub>2</sub> composite ceramics. *J. Alloys Compd.* **2015**, *643*, 88–93. [CrossRef]
32. Lazar, M.A.; Varghese, S.; Nair, S.S. Photocatalytic Water Treatment by Titanium Dioxide: Recent Updates. *Catalysts* **2012**, *2*, 572–601. [CrossRef]
33. Su, C.; Lin, K.-F.; Lin, Y.-H.; You, B.-H. Preparation and characterization of high-surface-area titanium dioxide by sol-gel process. *J. Porous Mater.* **2006**, *13*, 251–258. [CrossRef]
34. He, R.; Tsuzuki, T. Synthesis of high surface area amorphous tin-zinc oxides by a sol-gel method. In Proceedings of the 2010 International Conference on Nanoscience and Nanotechnology (ICONN 2010), Sydney, Australia, 22–26 February 2010; pp. 154–157. [CrossRef]
35. Nateq, M.H.; Ceccato, R. Sol-Gel Synthesis of TiO<sub>2</sub> Nanocrystalline Particles with Enhanced Surface Area through the Reverse Micelle Approach. *Adv. Mater. Sci. Eng.* **2019**, *2019*, 1–14. [CrossRef]
36. Picco, S.; Villegas, L.; Tonelli, F.; Merlo, M.; Rigau, J.; Diaz, D.; Masuelli, M. Sol-Gel Processes of Functional Powders and Films. 2016. Available online: <https://www.intechopen.com/books/chemical-reactions-in-inorganic-chemistry/sol-gel-processes-of-functional-powders-and-films> (accessed on 12 February 2021).
37. Ola, O.O.; Maroto-Valer, M.M.; Liu, D.; Mackintosh, S.; Lee, C.-W.; Wu, J.C.S. Performance comparison of CO<sub>2</sub> conversion in slurry and monolith photoreactors using Pd and Rh-TiO<sub>2</sub> catalyst under ultraviolet irradiation. *Appl. Catal. B Environ.* **2012**, *126*, 172–179. [CrossRef]
38. Yang, G.; Li, C. Electrofiltration of silica nanoparticle-containing wastewater using tubular ceramic membranes. *Sep. Purif. Technol.* **2007**, *58*, 159–165. [CrossRef]
39. Kuvayskaya, A.; Lotsi, B.; Mohseni, R.; Vasiliev, A. Mesoporous adsorbents for perfluorinated compounds. *Microporous Mesoporous Mater.* **2020**, *305*, 110374. [CrossRef]
40. Stebel, E.K.; Pike, K.A.; Nguyen, H.; Hartmann, H.A.; Klonowski, M.J.; Lawrence, M.G.; Collins, R.M.; Hefner, C.E.; Edmiston, P.L. Absorption of short-chain to long-chain perfluoroalkyl substances using swellable organically modified silica. *Environ. Sci. Water Res. Technol.* **2019**, *5*, 1854–1866. [CrossRef]
41. Da Silva, R.C.; Kubaski, E.T.; Tenório-Neto, E.T.; Lima-Tenório, M.K.; Tebcherani, S.M. Foam glass using sodium hydroxide as foaming agent: Study on the reaction mechanism in soda-lime glass matrix. *J. Non Cryst. Solids* **2019**, *511*, 177–182. [CrossRef]
42. ASTM C128-15. *Standard Test Method for Relative Density (Specific Gravity) and Absorption of Fine Aggregate*; ASTM International: West Conshohocken, PA, USA, 2015; Available online: [www.astm.org](http://www.astm.org) (accessed on 12 February 2021).
43. Mills, A. An overview of the methylene blue ISO test for assessing the activities of photocatalytic films. *Appl. Catal. B Environ.* **2012**, *128*, 144–149. [CrossRef]
44. Gurav, J.L.; Jung, I.-K.; Park, H.-H.; Kang, E.S.; Nadargi, D.Y. Silica Aerogel: Synthesis and Applications. *J. Nanomater.* **2010**, *2010*, 1–11. [CrossRef]
45. Şahin, I.; Özbakır, Y.; İnönü, Z.; Ulker, Z.; Erkey, C. Kinetics of Supercritical Drying of Gels. *Gels* **2018**, *4*, 3. [CrossRef]
46. Levy, D.; Zayat, M. *The Sol-Gel Handbook: Synthesis, Characterization, and Applications*, 1st ed.; Wiley-VCH Verlag GmbH & Co. KGaA: Weinheim, Germany, 2015.
47. Danks, A.; Hall, S.R.; Schnepf, Z. The evolution of ‘sol-gel’ chemistry as a technique for materials synthesis. *Mater. Horiz.* **2016**, *3*, 91–112. [CrossRef]
48. Available online: <http://www.iso.org/iso/isocatalogue/cataloguetc/cataloguedetail.htm?csnumber=46019> (accessed on 13 February 2021).
49. Nibret, G.; Ahmad, S.; Rao, D.G.; Ahmad, I.; Shaikh, M.A.M.U.; Rehman, Z.U. Removal of Methylene Blue Dye from Textile Wastewater Using Water Hyacinth Activated Carbon as Adsorbent: Synthesis, Characterization and Kinetic Studies. *SSRN Electron. J.* **2019**, 1959–1969. [CrossRef]
50. Hou, C.; Hu, B.; Zhu, J. Photocatalytic Degradation of Methylene Blue over TiO<sub>2</sub> Pretreated with Varying Concentrations of NaOH. *Catalysts* **2018**, *8*, 575. [CrossRef]
51. Mills, A.; Hazafy, D.; Parkinson, J.; Tuttle, T.; Hutchings, M.G. Effect of alkali on methylene blue (C.I. Basic Blue 9) and other thiazine dyes. *Dyes Pigment.* **2011**, *88*, 149–155. [CrossRef]
52. Milošević, M.D.; Logar, M.M.; Poharc-Logar, A.V.; Jakšić, N.L. Orientation and Optical Polarized Spectra (380–900 nm) of Methylene Blue Crystals on a Glass Surface. *Int. J. Spectrosc.* **2013**, *2013*, 1–6. [CrossRef]
53. Pennell, K. Transport and Remediation of Per- and Polyfluoroalkyl Substances (PFAS) in the Subsurface. In press.
54. Zhang, W.; Liang, Y. Removal of eight perfluoroalkyl acids from aqueous solutions by aeration and duckweed. *Sci. Total Environ.* **2020**, *724*, 138357. [CrossRef]